frontiers | Frontiers in Earth Science

TYPE Original Research
PUBLISHED 24 January 2024
DOI 10.3389/feart.2023.1281153

OPEN ACCESS

EDITED BY
Jie Liao,
Sun Yat-sen University, Zhuhai Campus, China

REVIEWED BY
Lijie Wang,
Guangzhou Marine Geological Survey, China
Zhongxian Zhao,
Chinese Academy of Sciences (CAS), China

*CORRESPONDENCE
Yuanyuan Liang,
liangyy18@cnooc.com.cn
Shi Chen,
chenshi4714@163.com

RECEIVED 22 August 2023
ACCEPTED 04 December 2023
PUBLISHED 24 January 2024

CITATION
Liang Y, Yang D, Chen S, Zhang G, Bai Z, Liang X, Wang Y, Wang L, Guo S, Ji M and Yan H (2024), The effect of the faults to the tectono-stratigraphy evolution in the Panyu low uplift.
Front. Earth Sci. 11:1281153.
doi: 10.3389/feart.2023.1281153

The effect of the faults to the tectono-stratigraphy evolution in the Panyu low uplift

Yuanyuan Liang[1]*, Dongsheng Yang[1], Shi Chen[2]*, Gongcheng Zhang[1], Zhizhao Bai[1], Xinxin Liang[2], Yunuo Wang[1], Long Wang[1], Shuai Guo[1], Mo Ji[1] and Hui Yan[3]

[1]CNOOC Research Institute Ltd., Beijing, China, [2]College of Geosciences, China University of Petroleum, Beijing, China, [3]Shenzhen Branch, CNOOC, Shenzhen, China

Introduction: The Panyu low uplift is located in the middle of the Central Uplift Belt of the Pearl River Mouth Basin, which has experienced multiple episodes of tectonic movements since the Cenozoic, and the faults are extensively developed there. The fault activities had a significant influence on the migration and accumulation of oil and gas, as well as the sedimentation.

Methods: In order to recognize the effect of the faults on the tectono-straigraphy evolution in the Panyu low uplift, based on the high-resolution seismic and latest drilling well data, the study has comprehensively analyzed the geometry and kinematics of these faults, as well as the sedimentary filling evolution of the residual depressions.

Results: The results show that two major fault systems has developed in the Panyu low uplift: the deep and shallow fault systems. The former was dominated by a series of NEE and NW-trending high-angle listric/plane faults, along with several low-angle detachment normal faults, which were under the joint control of the NW-SE and NS-trending extensional stress during the Eocene. The latter was dominated by NW-NWW trending strike-slip normal faults with tension-shear properties under the NEE trending dextral strike-slip stress field in the late Miocene. The uplift had undergone five tectonic evolution stages: the initial rifting stage (Tg-T83), the intensive rifting stage (T83-T80), the rifting and depression transitional stage (T80-T70), the thermal subsidence depression stage (T70-T35), and the tectonic reactivation stage (T35-T10).

Discussion: Based on the 3D seismic phase interpretation and drilling sample analyses, the study also indicates that during the initial rifting stage, the Panyu low uplift manifested as multistage depositional center. The sedimentary strata were distributed in the downthrown wall of the depression-controlling faults, exhibiting multiple subsidence and sedimentary centers, and the depressions was supplied by multi-provenance systems. During the intense rifting period, the depression widened, the lacustrine basins were connected with each other, and the sedimentary center migrated. During the rifting and depression transitional stage, the faults controlling on deposition weakened. The thick Enping formation from the northwest provenance direction is unconformably overlaid on the Panyu low uplift. Meanwhile, the depressions was characterized by the sedimentary deposits of lacustrine basin. Various types of sedimentary facies were developed, including the delta, semi-deep lacustrine, shallow lacustrine, and

shore-shallow lacustrine deposits, and the mudstone of the semi-deep lacustrine facies could serve as a high-quality source rock for the hydrocarbon production.

KEYWORDS

residual depression, tension-shear fault, tectonic evolution, Panyu low uplift, Pearl River Mouth Basin, sedimentary filling

1 Introduction

As one of the most important oil and gas enrichment area in the South China Sea, the Pearl River Mouth Basin (PRMB) plays a crucial role in the oil and gas industry (Pang et al., 2008; Zhu et al., 2012; Zhu et al., 2012; Pang et al., 2014; Shi et al., 2014; Sun et al., 2014; Zhang et al., 2014; Mi et al., 2019; Dai et al., 1998; Gong et al., 1997; Zhang et al., 2023; Zhu et al., 2012; Zhu et al., 2015). The Pearl River Mouth Basin is located in the northern continental margin of the South China Sea and shows two major exploration fields: shallow water (water depth<300 m) and deep water field (water depth>300 m). From north to south, it is divided into "three uplifts and two depressions" of NE trending. The depressions in the shallow water area consist of the Zhu I and Zhu III depressions, while the depressions in the deep water area consist of the Zhu II and Zhu IV depressions (Figure 1A).

The study area, the Panyu low uplift, has its unique geological features, such as its position within the basin and its relationship to the surrounding structures, that contribute to its status as a prime area for oil and gas accumulation. Since 2001, represented by the LH19-3, LH19-1, PY30-1, and PY35-1, a serious number of gas fields and gas-bearing structures have been discovered in the uplift (Mi et al., 2006; Wang et al., 2005; Yu et al., 2007). Extensive research has been done on the tectonic evolution and deposition of the Pearl River Mouth Basin, most of which have focused on the level of large-scale basins (Pang et al., 2008; Mi et al., 2019; Pang et al., 2021; Xia et al., 2018), especially in the Baiyun Depression, Shenhu, and Dongsha Uplift. As for the Panyu low uplift area, past studies concentrated on the relationship between the late-stage faulting activities and hydrocarbon accumulation (Yu et al., 2007; Wang, 2007; 2005; Zhang et al., 2011), as well as the sedimentary evolution and filling characteristics of residual depressions (Xue et al., 2012; Zong et al., 2012; Wang et al., 2023). At present, a systematic research on the fault activities of the Panyu low uplift and its effect on the tectono-stratigraphy is still lacking.

The Panyu low uplift is unique in its structural location, being sandwiched between the Zhu I and Zhu II depressions. The depression structure revealed by the seismic profile is consistent with typical rifted basins in the Zhu I depression, which is dominated by grabens and half-grabens stuctures controlled by high-angle normal faults (Liu et al., 2018; Xie et al., 2009). While the Zhu II depression is considered to be a wide and deep rifted depression controlled by a low-angle large detachment fault system. At first, the Panyu low uplift, as a transitional area between the Zhu I and Zhu II depressions, was considered to be the same as the Zhu I depression, which was characterized by brittle deformation. During the rifting period, it showed typical rifted basin structures without detachment characteristics. In fact, with the deepening of exploration, especially the drilling of a large number of deep-water wells and the interpretation and processing of high-resolution 3D seismic data, a large number of magmatic rocks and pre-existing faults have been identified in the Pearl River Mouth Basin, including the Zhu I depression (Ye et al., 2018; Deng et al., 2019; Xie et al., 1989). And there's a large amount of evidence proved that magmatic activities and pre-existing faults had participated in the transformation of the structures of rifted basins, making the structural styles of the basin diverse and complex (Pang et al., 2021). Therefore, the previous point of view that there were only rifted structures controlled by simple high-angle plate normal faults in the Panyu low uplift still needs to be further investigated. In

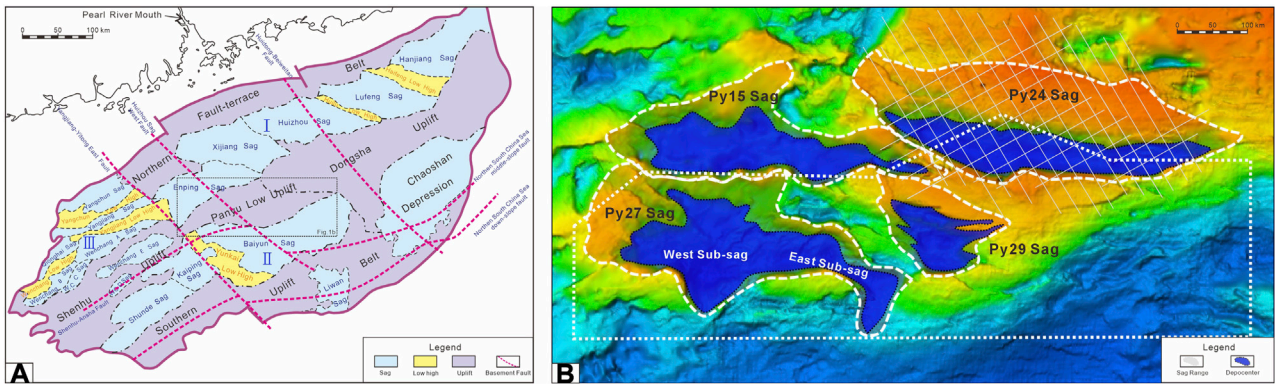

FIGURE 1
(A) Map of main structural units in the Pearl River Mouth Basin (after Dong et al., 2008; Zong et al., 2012; Ma et al., 2022). I--Zhu I depression; II--Zhu II depression; III--Zhu III depression **(B)** Location of the Panyu low uplift in the PRMB with divisions of tectonic units.The white lines show the distribution of the 2-D seismic lines. The irregular border denotes the scope of the 3-D seismic survey.

addition, the structural style of the depressions controls the sedimentary geomorphological characteristics and, thus, the type of sedimentary systems. Since the division of the tectonic evolution stages and the corresponding stratigraphic distribution characteristics are not well correlated, a reasonable model for the evolution of tectonic activities and sedimentary filling is necessary.

In view of this, based on the high-resolution 3D and 2D seismic data, regional geological background, and the latest well drilling data, by means of fault system analysis, sedimentary structure filling analysis, and structural evolution recovery, the study aimed to 1) study the geometric characteristics of faults in the uplift in both planar and longitudinal directions, analyze the fault types and the combinations between them; 2) characterize and analyze the regional unconformity and straitigraphic distribution. Combined with the fault kinematics, study the spatiotemporal evolution of corresponding strata and reconstruct the control of tectonic activities on sedimentation during different evolutionary stages; 3) put the new information into an evolutionary framework to reveal the tectonic evolution process and development model of the Pearl River Mouth Basin. In addition, this research can also provide a theoretical support for studying the distribution of potential source rocks in the residual depressions of uplifts of the PRMB, which further assists in the exploration of hydrocarbons in this region.

2 Geological background

The South China Sea (SCS) is located to the southeast of the Eurasian continent and is one of the largest marginal seas in the west Pacific Plate. And the PRMB, located in the northern continental margin of the SCS, spans an area of over 200,000 km^2 and is regarded as one of the most petroleum-rich basins in China. Controlled by the NE/ENE and NW-striking regional deep faults, the PRMB presents an elongated block pattern in the NE and NW directions, respectively. Previous studies have divided the PRMB into five structural provinces, including the Northern Fault-Terrace Belt, the Northern Depression, the Central Uplift, the Southern Depression, and the Southern Uplift Belt (Figure 1A). And the research area, the Panyu low uplift, is located in the central part of the Central Uplift Belt, which belongs to a secondary positive structural unit of the uplift belt. In plain view, this NE trending uplift presents an irregular rhombic shape with an area of approximately 8,350 km^2 and a water depth of 100–200 m (Figure 1B).

The basement prototype of the Pearl River Mouth Basin is considered to be a combination of continental marginal magmatic arc, fore-arc basin, and foreland basin, formed by the intense compression of the Eurasian plate in response to the Paleo-Pacific plate's subduction into the continental crust of the Eurasian plate in the NNW direction during the Mesozoic (Zhou et al., 2005a; Zhou et al., 2005b; Zhou et al., 2006; Zhang et al., 2015). The retreat of the paleo-Pacific plate subduction in the late Mesozoic led to the back-arc spreading of the southeast margin of the Eurasian plate. As a result, the northern continental margin of the South China Sea, where the Pearl River Mouth Basin was located, underwent rifting and extensional stages (Zhou et al., 2002; Chen et al., 2005). This tectonic activity lasted until the Eocene, when the Indian plate and the Eurasian plate continued to collide. During this period, the Pearl River Mouth Basin experienced the Shenhu Movement (about 55 Ma), the Zhuqiong I Episode (about 43 Ma), and the Zhuqiong II Episode (about 38 Ma; Chen et al., 2003; Gong et al., 2004; Pang et al., 2008; Ren and Lei, 2011; Pang et al., 2014; Zhong et al., 2014; Zhang, 2010; Zhu and Lei, 2013). The basin began to enter the evolution stage of the intracontinental syn-rift phase, where the upper and lower Wenchang formations and the Enping formation were successively deposited. About 32 Ma ago, the northern continental margin of the South China Sea experienced the South China Sea movement, which led to the breakup and seafloor spreading of the central basin of the SCS (Xie et al., 2015). The northern continental margin of the SCS entered the post-rift stage. The basin was dominated by regional overall subsidence, while considerable post-breakup extensional deformation was recorded in the continental margins of the SCS. Numerous normal faults have developed during continental breakup in the SCS margin, e.g., in the Pearl River Mouth Basin (PRMB) (Sun et al., 2014; Ye, 2019). The Baiyun sag had undergone at least three episodic tectonic events during the syn-spreading stage (Deng et al., 2018). During this stage, the Zhuhai, Zhujiang, and lower Hanjiang formations were deposited in the basin (Liu et al., 2011; Pang et al., 2018). Since the late Miocene (approximately 13.8 Ma), the Philippine plate wedged into the Eurasian and Pacific plates, and NW compressive stress was transmitted to the basin, which is characterized by the uplift and denudation of the Dongsha uplift and the extensive development of a large number of tension-shear faults in the PRMB (Sun et al., 2014; Ren et al., 2018; He et al., 2019; Zheng et al., 2022). During this period, the upper Hanjiang and Wanshan formations were deposited.

According to the latest borehole and seismic data, the Cenozoic formations are integrated from bottom to top in the Panyu low uplift: the Wenchang, Enping, Zhuhai, Zhujiang, Hanjiang, Yuehai, Wanshan formations, and the Quaternary (Figure 2). The stratigraphic successions are divided by the second-order sequence interfaces Tg, T80, T70, T60, T40, T35, T32, and T20, respectively. Besides, third-order sequence boundaries T83 (WCSB4), T50 (MFS18.5), and T35 (SB13.8) can also be identified within the stratigraphic sequences (Dong et al., 2008; Zhao et al., 2009; Liu et al., 2011; Xue et al., 2012; Zong et al., 2012). The Wenchang formation is mainly composed of grayish-black lacustrine mudstone, distributed in the depressions in the uplift locally. And the Enping formation has a wider distribution than the former. It is dominated by the gray interbedded mudstone and sandstone of delta, fluvial, and swamp facies. The lithological assemblages of the Zhuhai and lower Zhujiang formations are similar; they are dominated by gray mudstone, fine-medium sandstone, and thin-bedded limestone of transitional facies and delta facies. The upper Zhujiang formation is dominated by gray, arenaceous mudstone interbedded with siltstone, and the depositional environment is a continental shelf. The Hanjiang-Yuehai formation, also formed in the continental shelf environment, consists of interbedding mudstone, arenaceous mudstone, and laminated calcareous mudstone, intercalated with fine-medium sandstone.

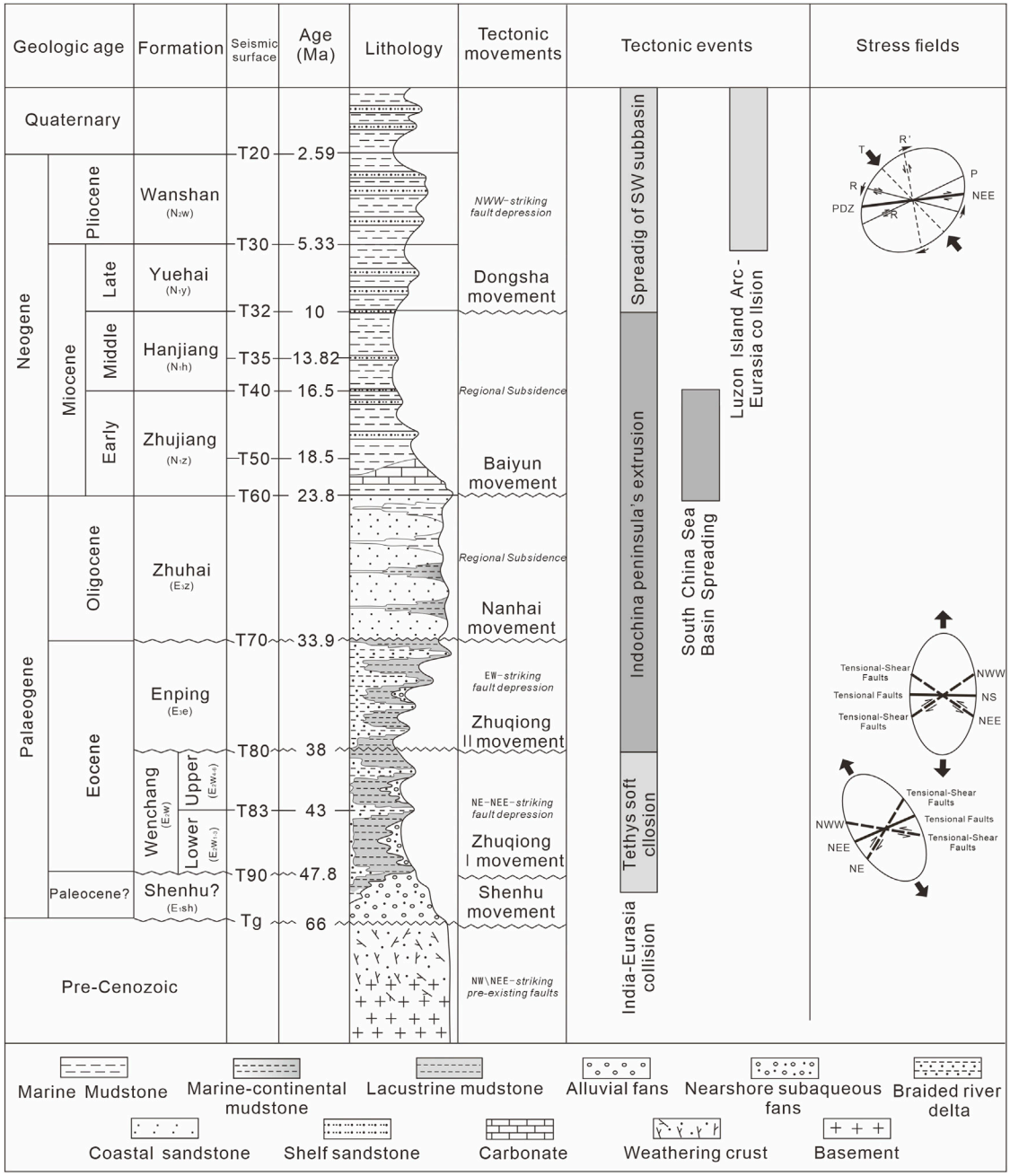

FIGURE 2
Chart showing the Pearl River Mouth Basin stratigraphy, the seismic reflecting surfaces (horizons), and the timing of regional tectonic movements (After references Shi et al., 2014; Briais et al., 1993; Li et al., 2014, slightly modified).

3 Data and methodology

High-quality 3D seismic data acquired by the Shenzhen Branch of CNOOC was used for the detailed interpretation and characterization of the faults and horizons distributed across the Panyu low uplift (Figure 1B). In addition, a series of NW and NE-directed regional 2D seismic lines were also used to clarify the distribution of the PY24 depression beyond the coverage area of 3D seismic data. The seismic streamers were 6 km long with 480 channels with a channel interval of 12.5 m. The frequency was 25 Hz, and the vertical resolution was 5–60 ms. Besides, a large amount of borehole data was used to provide the lithological information for stratigraphic horizon calibration, which was also used to make the thickness map.

The fault geometry is described in detail in both the inline and crossline directions, with a spacing of 250 m*250 m based on the 3D seismic data across the uplift. The seismic coherence technique (Bahorich and Farmer, 1995) was also used to image the fault-

induced discontinuities, which greatly facilitated the identification of individual faults. Depth contour maps of two major seismic reflection layers (Top Basement, Top Lower Zhujiang formation) were carefully mapped to describe the fault geometries and styles in the plain. Besides, the Rose diagrams of fault strikes were used to synthetically analyze the spatiotemporal evolution of faults from the Paleocene to the Miocene. Morever, a key technique, the balanced section technique, which was widely applied in rift basins to reconstruct the evolutionary history of basins and to calculate the stretching factors by faults and other extensional-related parameters, was also adopted in this study (Gibbs, 1983; Williams and Vann, 1987; Groshong, 1989). In conjunction with this technology, we effectively improved the accuracy of profile interpretation and recovered the paleo-structural characteristics during the key period.

4 Characteristics of fault systems

Based on the 3D seismic data processing and multi-horizon coherence, the geometric and kinematic characteristics of faults in the Panyu low uplift were described in detail, and the fault active periods were defined. Affected by multiple episodes of tectonic movements, especially the joint action of the extensional stress generated by the Eocene Zhuqiong movement and the strike-slip stress generated by the Miocene Dongsha movement, faults are well developed across the Panyu low uplift. There are nearly 500 faults distributed in the uplift, forming a fault system dominated by NW, NWW, and NEE-trending normal faults with tension-shear properties. Based on the faults scales and the control on sedimentation, the faults in the low uplift can be divided into two major systems, which are the deep and shallow fault systems. The former is dominated by the large depression-controlling boundary faults, which have significant control on the deposition of uplift depressions during the period of fault activities. These type of faults were formed at an earlier stage, especially during the Paleocene-Eocene, controlling the subsidence of the depression in the uplift during that period, and some of them remained active until the late Neogene. The latter is formed at a later stage during the late Miocene-Quaternary. The faults in the shallow system are small in scale but large in number, representing an echelon or reverse "S" shape stepping pattern in plan view with a certain strike-slip component. In the shallow system, the faults that formed at the late stage usually dredge and control the oil and gas accumulation in the Zhujiang reservoirs of the study area (Shi et al., 2008; Zhang et al., 2011; He et al., 2019).

4.1 Characteristics of deep depression control faults

The deep depression controlling faults of Panyu low uplift are primarily dominated by a series of normal faults with listric or planar fault surface. The former was usually characterised by a decreasing dip angle with depth (Shelton, 1984), with the curved surface concave towards the top. Besides, several small-scale detachment faults can be observed among these normal listric faults, with a distinct pattern according to Davis et al., 2002, characterised by an initial dip of less than 30°. Formed in the early Eocene, the deep fault system were represented by the Panyu 27, Panyu 29, Panyu 24, and Panyu 25 sub-fault systems. These faults mainly trend in a NEE and NW direction and are distributed over a long distance in plain view, ranging from 12 km to 95 km. They exhibit dominated northward dipping in the seismic profile with a listric or rotating plane. Most of them were mainly in a large scale, cutting through the pre-Paleogene basement to the Cenozoic sediments from the bottom to up. The depressions controlled by the faults represent a half-graben structure, with the sedimentary strata overlapping to the north (Figure 3).

The Panyu 27 fault system consists of three NEE trending faults and two NW trending transfer faults with a serrated shape. The F2 and F3 faults controlling the western and eastern 1 sub-depression are both simple listric faults, merging with multiple secondary faults derived from the hanging wall and forming a complex "broom-like" structural style, making the sedimentary structures inside the depression more complicated (Figures 4A,B). To the east, the fault plane dips gently and is almost horizontal, with a dip angle of around 6°. The fault as a whole exhibits the structural style of a low-angle detachment normal fault. The seismic reflection reveals a fault plane that undulated, causing the arched deformation of the overlying strata. Besides, stepped normal faults developed on the hanging wall of the detachment fault control the rotation of multiple fault blocks, resulting in the formation of half-grabens with a domino shape. These small secondary normal faults cut into the basement surface and converge downward to the detachment surface. The horizontal sliding amount is relatively small, with a maximum of about 0.8 km. These faults mainly control the deposition of the Upper Wenchang formation. Most of them penetrate the strata near the T80 interface, and some faults have penetrated the strata of the Hanjiang formation since their long-term activity (Figure 4C). In addition, a large number of layered and upward-swelling seismic reflection characteristics can be observed in the basement around the Panyu 27 depression. These structures have significantly different seismic amplitudes compared to their surrounding rocks and are assumed to be magmatic underplating that forming during the rifting stage. These underplating structures would affect the structural deformation of the overlying strata and faults to some extent.

The Panyu 29 fault system is composed of three parallel faults that are nearly EW and NWW trending. The faults F8 and F9 to the north, which control the depression in the north, both show distinct reflection characteristics in the profiles and exhibit a low and gentle slope. They terminate at the T83 reflection interface and penetrate significantly deep into the basement. Affected by the fault occurrence, the sedimentary strata of the Lower Wenchang formation in the fault hangingwall steepen towards the gentle slope zone of the depression, with obvious flexure characteristics. In addition, a set of X-shaped conjugate faults and reverse faults have developed on the hanging wall of the F9 fault, which were formed at a later stage and cut into the shallow strata. Significantly different from the former, The F7 fault to the south shows a large, steep fault plane, which cuts through the basement and shallow cover layer. It cuts through the Paleogene to Quaternary strata, and its apex is close to the seafloor-T0 interface. Besides, it has significant control over the deposition of the Upper Wenchang and Enping formations. The strata adjacent to the fault root display a notable increase in thickness (Figure 5A), correspoding to the effect of the fault on the stratigraphic deposits of the time.

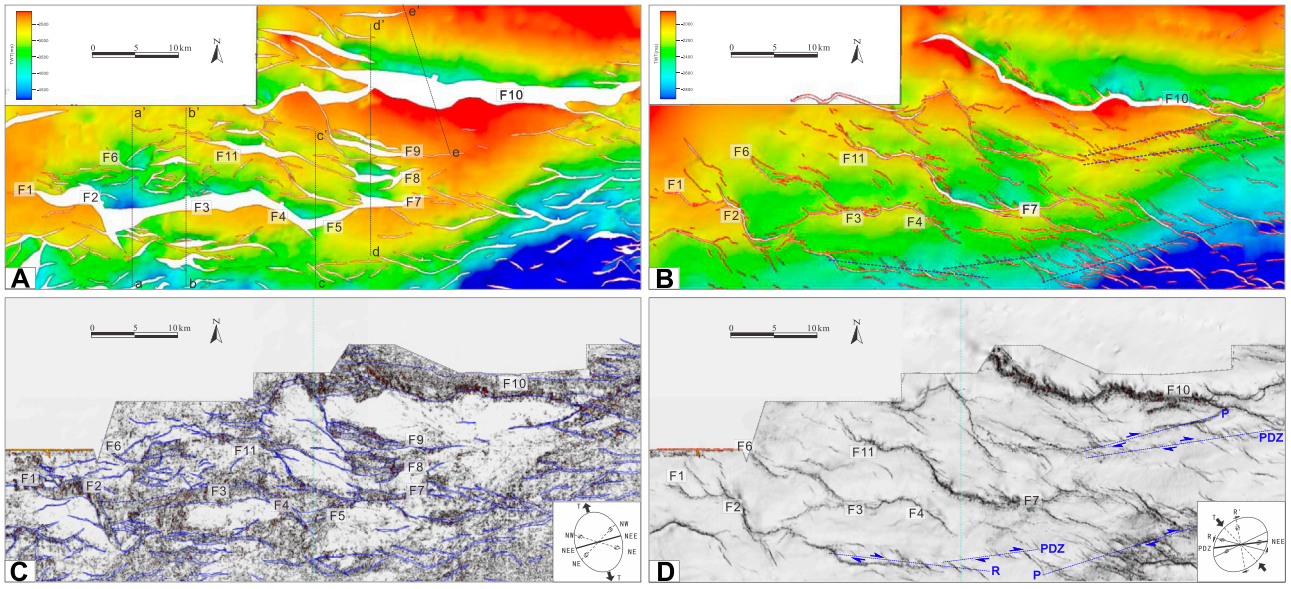

FIGURE 3
Map showing detailed geometries and distribution of faults in the study area. **(A,B)** Structural maps of the Tg and T50 surfaces with faults in the Panyu low uplift. **(C,D)** Coherence slices of surface Tg and T50 and the faults interpretations. The Mohr's circle in the right corner shows the direction of the stress field at particular period of time.

In contrast to the preceding two fault systems, the structural style of the Panyu 24 fault system is relatively simple. In plan view, it strikes in an approximately EW direction and intersects with the eastern branch of the Panyu 15 fault to the west (due to the incomplete 3D seismic data, the Panyu 15 fault system is not fully portrayed). The fault exhibits a solitary fault plane in its central while secondary faults occurr at the tips of the major fault, situated at both eastern and western sides, and shows a NW trend that differs from the major fault. Through the seismic profile, the Panyu 24 fault has a relatively steep occurrence with a dip angle of about 70°, which lessened gradually towards deeper layers until it retreated into the bedrock (Figure 5B). A notable reverse traction structure is observed in the hanging wall of the fault, resulting from the gravitational drag during the sliding of the strata in the hanging wall under extension. Additionally, accompanying secondary faults are formed, intersecting with the main fault in a "Y" shape, where the area of insufficient toughness.

In addition to the normal faults that cut through the sedimentary cover, some low-angle residual thrust faults are also identified in the basement. The thrust faults exhibit distinct occurrences compared to later-formed normal faults, terminating at the Tg reflection layer. Using seismic, gravity, and magnetic interpretation, two groups of NE and NWW trending thrust faults and NW trending strike-slip fault zones have been identified in the basement structural layer in the Pearl River Mouth Basin (Song et al., 2002; Liu et al., 2018; Luo et al., 2018). Additionally, intermediate-basic magma is distributed along this strike-slip fault zone at the post-rift stage (Chen et al., 2005; Zhou and Yao, 2009; Sun et al., 2014; Lu et al., 2015; Ye, 2019). Since the proximity of pre-existing faults belongs to a mechanically structural weak zone, they can serve as weak zones during structural deformation. In the superimposed stress field at the late stage, tectonic activation is prone to occur along the fracture plane (Holdsworth et al., 2001; Morley et al., 2004; Pang et al., 2021). The previous studies show that the basement pre-existing structure usually has a profound effect on the tectonic evolution of the entire basin at the late stage, such as the Tarim, Junggar, and Bohai Bay Basins in China (Ma et al., 2008; Qiu et al., 2019; Liu et al., 2023). For instance, the formation and development of the NE trending strike-slip fault system in the Shunbei region of the Tarim Basin are controlled by the underlying weak zone of the NE trending pre-existing basement structural and differential pushing and basement shear effect under contractional stress (Han et al., 2017; Ning et al., 2018; Jia et al., 2022). Likewise in the PRMB, previous research shows that a group of NE trending with northward dipping low-angle faults had developed in the basement of the Panyu low uplift and its surrounding area. Based on the regional tectonic setting, it was assumed that this was a product of Mesozoic NW-SE compressive stress (Wang et al., 2023). Some depression controlling faults with low angles in the study area, such as the eastern section of the Panyu 27 fault and the northern part of the Panyu 29 fault system, might have undergone tectonic reactivation in response to the extensional stress of different directions on the basis of pre-existing thrust faults.

4.2 Characteristics of shallow tension-shear faults

Most shallow faults have an inheritance with the early-formed faults in terms of spatial distribution and activity characteristics, while a few newly formed faults are independently distributed from the deep fault system and sporadically developed around the periphery of the Panyu low uplift. On the plane, most faults are NW-NWW and near EW trending and consist of multiple sets of en

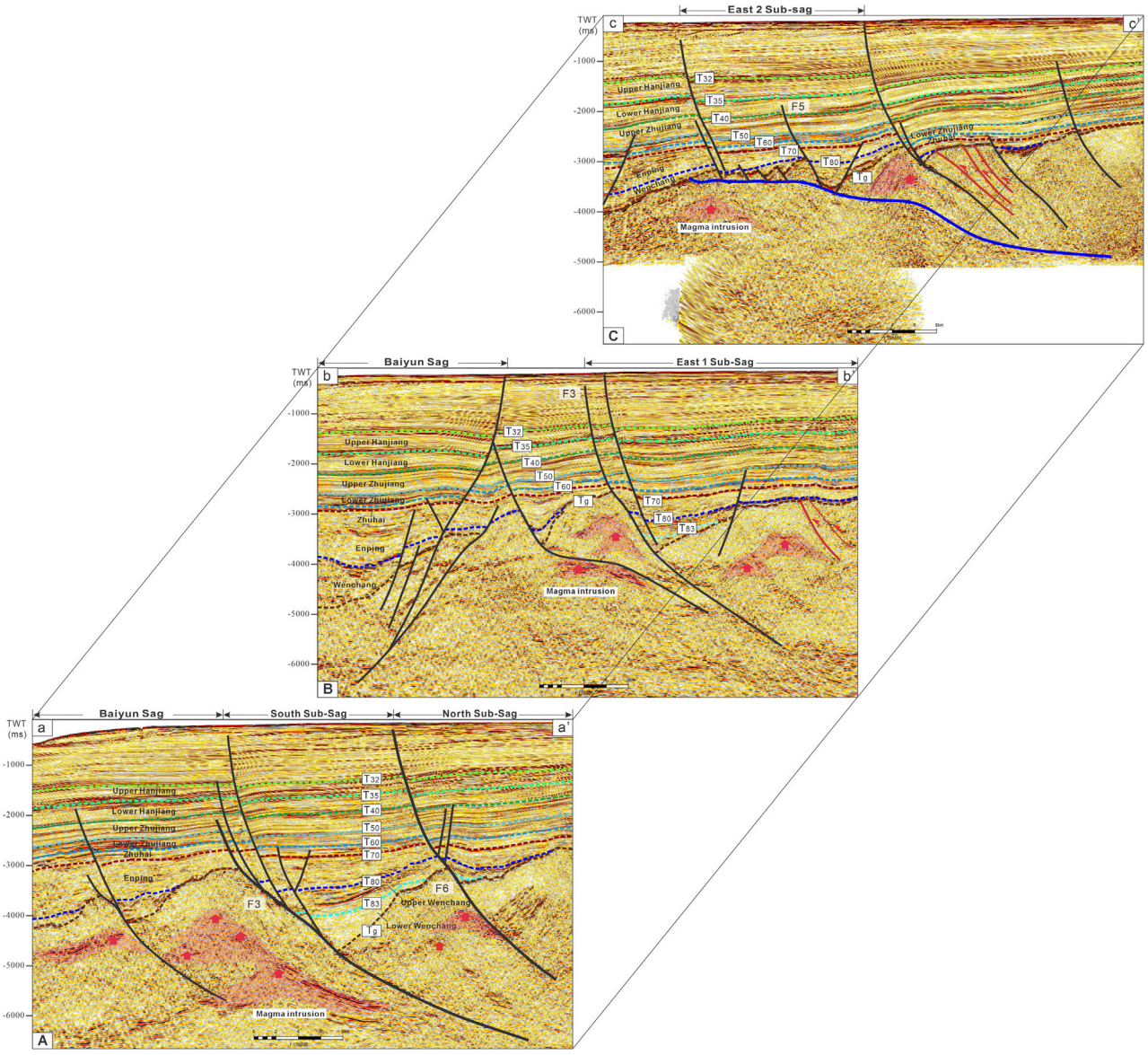

FIGURE 4
Interpreted seismic profiles **(A)** a-a′, **(B)** b-b′, and **(C)** c-c′ across PY27 sag in the Panyu low uplift area (locations are shown in Figure 3A).

echelon and reverse "S"-shaped fault zones (Figure 3B). The shallow faults exhibit prominent strike-slip characteristics. Most of them gradually transition from relatively continuous faults in the deep to a series of strike-slip fault zones consisting of a series of secondary faults that overlapped back and forth. For instance, a typical extensional strike-slip fault zone presenting in "S-shaped" PDZ was finely delineated in the central region of the study area, corresponding to the F7 and F11 normal faults located in the deep strata. The fault system inherently developed on the deep structure and evolved into four geometric segments that overlap each other. The strike of the master fault changes abruptly, ranging from N89° to N177° from west to east. The associated secondary faults on both sides of the main fault are small in scale and dense in distribution. They are obllique to the primary fault at an acute angle, with a length of 2–4 km (Figure 6C). On the seismic profile, these faults break from the T20 seismic reflection interface to the deep basement. Among them, in terms of the fault displacement, the F4 fault has significantly larger displacement in the basement than in the shallow cover layer. It reactivated on the basis of a pre-existing listric normal fault, forming a negative flower structure together with other late-formed sub-faults. In addition, based on the coherence attribute, several sets of en echelon fault zones with inconsistent strikes are observed on the eastern and southern sides of the uplift (Figure 3D). The fault zones are mainly distributed in NEE and NWW direction. The en echelon structure is a common planar identifier of strike-slip fault system, and the individual faults that consists of the echelon fault zones has similar fault strikes and exhibits left-step geometric features in the map view (Figure 6D). The fault planes are steep, representing a parallel or conjugate distribution in the section (Figure 6A).

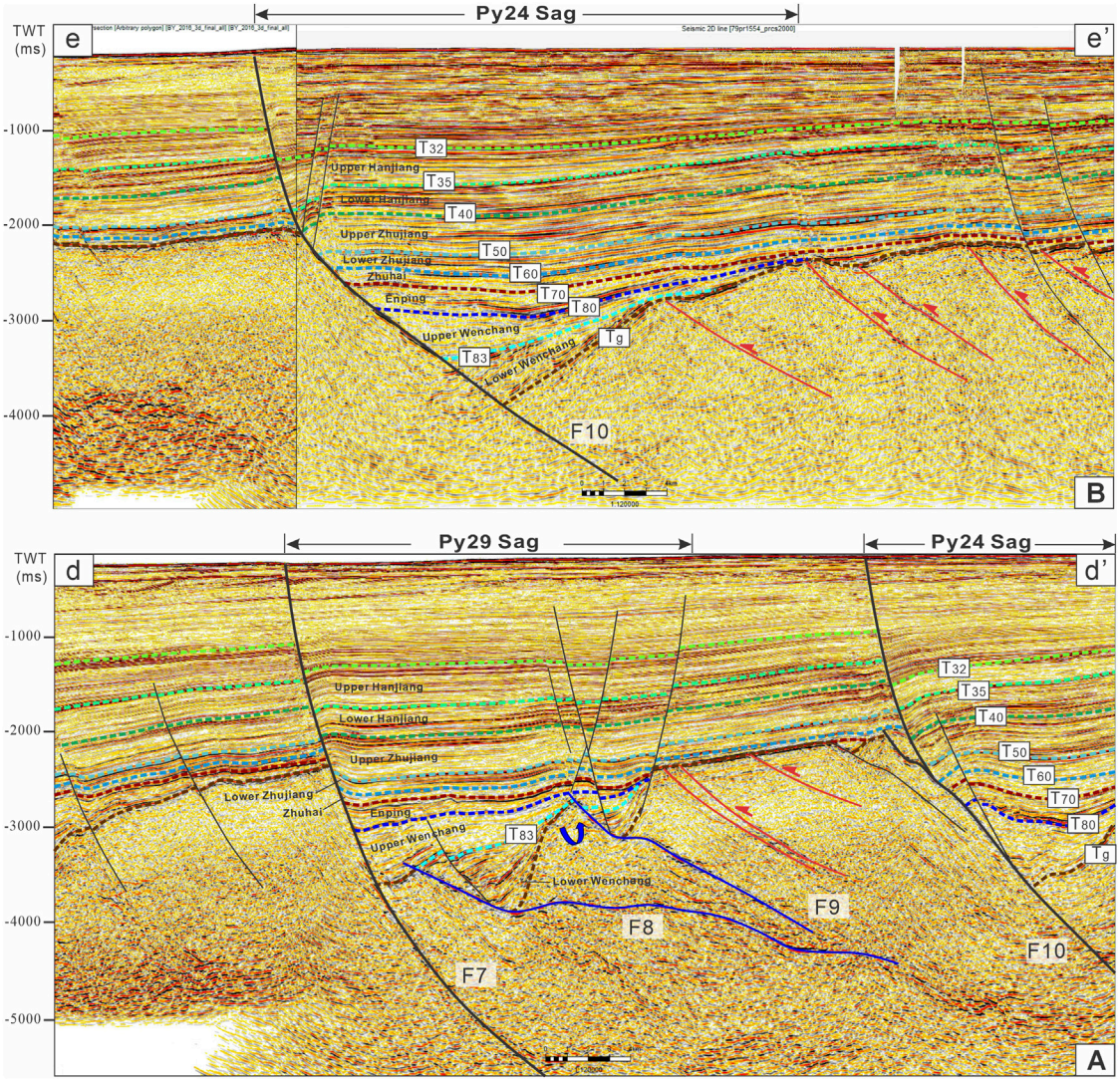

FIGURE 5
Interpreted seismic profiles **(A)** d-d′, **(B)** e-e′ across PY24 and PY29 sags in the Panyu low uplift area (locations are shown in Figure 3A).

Horsetail-like structures (also known as broom-like structures) can also be observed in the study area. They are characterized by a series of secondary faults spreading in the NW direction at the end of the main fault. The fault strike of individual faults with the hosetail-like structure is same as other secondary faults in the main fault zone (Figures 6B,C). Based on the geometric features and arrangement pattern of the late-formed tension-shear faults, as well as the displacement direction of the strata on both sides of faults (on the plane), it is inferred that these faults have dextral movement characteristics.

5 Tectonic evolution

The deep water area in the northern South China Sea, where the Panyu low uplift is located, is at the junction of the Eurasian, Pacific, and Indo-Australian plates. Its tectonic evolution is controlled by tectonic events such as the retreat of the Pacific plate, the uplift of the Qinghai-Tibet Plateau, the expansion of the South China Sea, and the subduction of the Philippine plate (Hall, 2002; Han et al., 2016; Li et al., 2012; Luo et al., 2018). Since the Paleogene, it has undergone multiple episodes of tectonic movements, such as the "Shenhu Movement, Zhuqiong I Episode, Zhuqiong II Episode, South China Sea Movement, Baiyun Movement, and Neotectonic Movement" (Ru, 1988; Li, 1993; Liu and He, 2001; Zhou et al., 2005a; Sun et al., 2005; Pang et al., 2007; Dong et al., 2008; Zhang et al., 2018; Ma, 2020; Clift and Lin, 2001; Bao et al., 2013; Cheng et al., 2013). The superposition and transformation of different episodes of tectonic movements have led to a complex and variable regional stress environment. At the early stage in Eocene, the regional extensional stress field transitioned from NW-SE trending clockwise dextral extension to nearly NS trending extension. During the late Miocene, it transitioned to strike-slip stress field of the NEE trend, which is derived from the horizontal compressive stress of NW-trending. Correspondingly, the dominant distribution direction of the

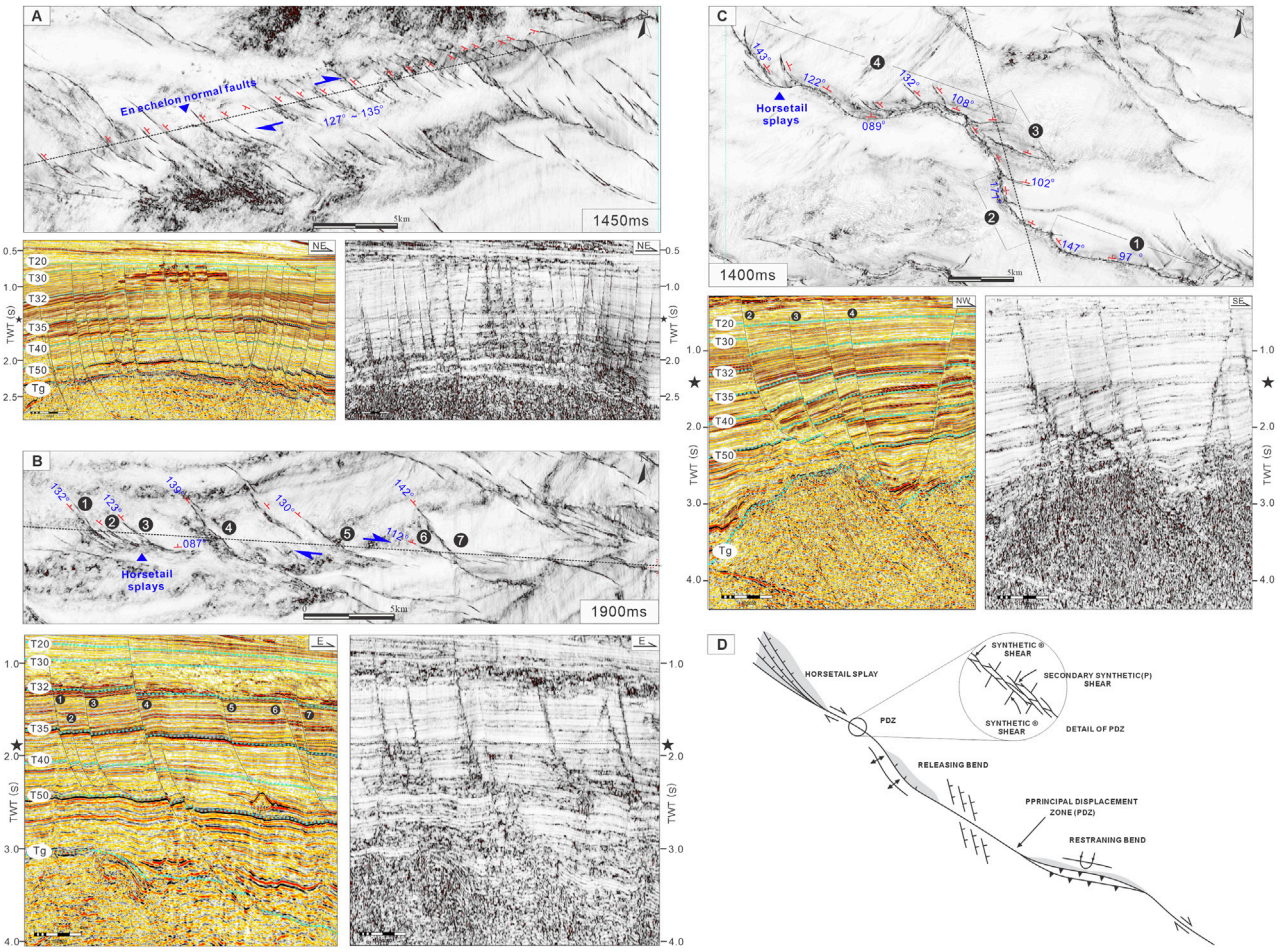

FIGURE 6
(A–C) Typical interpreted coherence slices and seismic profiles of the shallow tension-torsional fault system. The uninterpreted images at the lower right corner are shown for comparison. The location of sections are labeled in black dotted lines **(D)** The spatial arrangement of structures associated with an idealized right-slip fault in the plain view (after reference Christie-Blick, 1995).

derived faults transitioned from NEE trending clockwise rotating to NW-SE trending (Figure 7). The geometric development characteristics of the fault system has demonstrated the superimposition influence of extension and strike-slip stress fields in the Panyu low uplift, and the spatiotemporal differences in fault activities result in the complex and diverse structural characteristics of the basin. As a result, based on the distribution characteristics and activity of the faults, as well as the contact relationship between strata, the overall development and evolution of the Panyu low uplift were divided into five tectonic evolution stages, including the initial rifting stage, the intense rifting stage, the rifting and depression transitional stage, the thermal subsidence depression stage, and the tectonic activation stage.

During the initial rifting stage (Tg-T83), under the joint control of the NW-SE trending extensional stress and the pre-existing NE trending basement faults, a series of NEE and NW trending depression control faults developed within the uplift (Figures 8A, B). Since the rose chart revealed that the maximum dominant strike of the fault was about N85°, it was inferred that the basin was controlled by NEE-trending faults. Especially in the western and central Panyu 27 depression, the northern Panyu 29 depression, and the Panyu 24 depression, the narrow half-graben was significantly controlled by high-angle faults (Figure 8B). During the intense rifting period (T83-T80), the maximum dominant strike of the fault was approximately N87° and N102° (Figure 7F). The extension was further strengthened, and all sub-depressions deepened and widened on the basis of the primary fault depression pattern. On the eastern side of the Panyu 27 depression, the pre-existing thrust fault in the basement served as a relatively weak surface in the extensional stress field at the late stage, forming small-scale extensional detachment faults under intense extension. The domino-type normal faults in the hanging wall controlled the development of the sedimentary strata in the eastern sub-depression. And the extensional deformation intensity was close to the western sub-depression. In the Panyu 29 depression, the depression control faults migrated southwards, causing the sedimentary center to migrate to the south as well. As a result, the early-formed fault depression tilted and rotated, forming a clear angular unconformity between the lower and upper Wenchang formations (Figure 8C). At the same time, magma intrusion took place at multiple locations in the Panyu low uplift (Figure 4). On the one hand, the continuous intrusion of magma slowed down the deformation of adjacent faults and strengthened the extension and

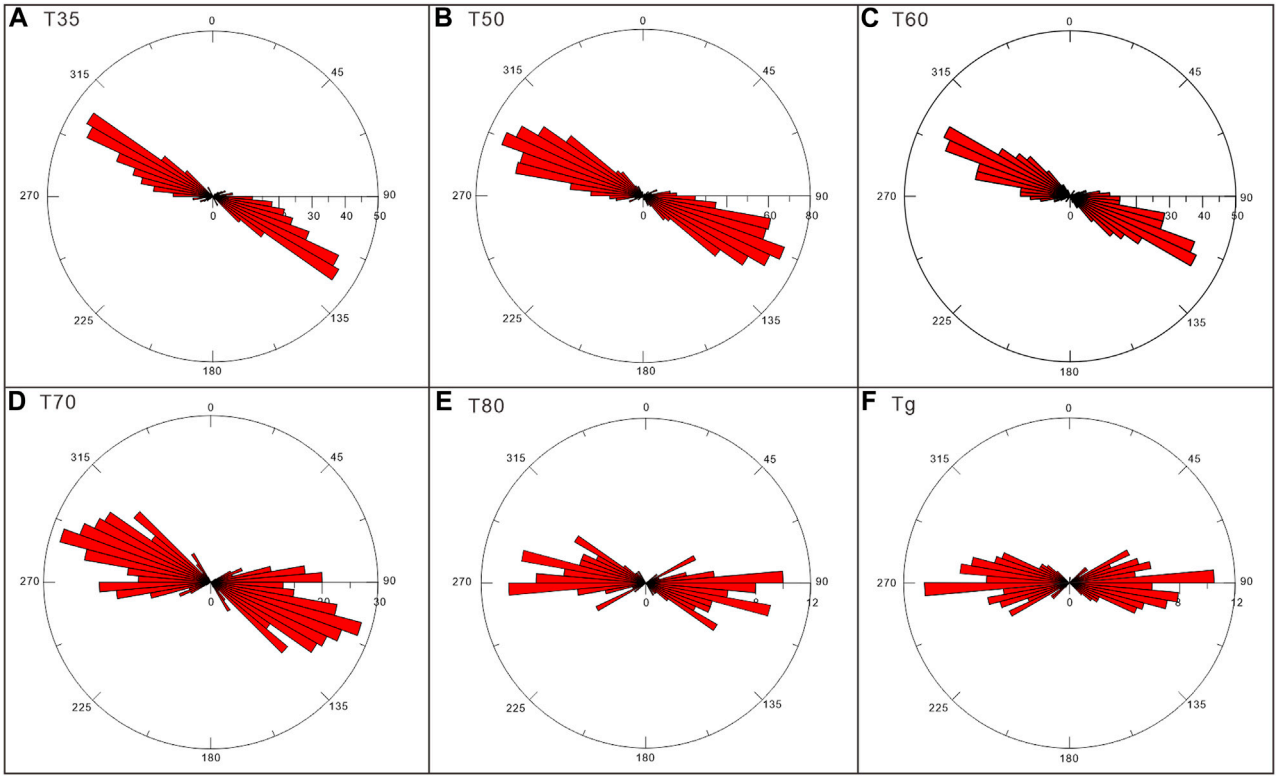

FIGURE 7
Rose diagrams of **(A)** T35 **(B)** T50 **(C)** T60 **(D)** T70 **(E)** T80 and **(F)** Tg seismic reflector of the faults in the Panyu low uplift.

thinning of faults. On the other hand, the strata in the gentle slope zone of the deep depression were uplifted and tilted by the magma, while the side near the main control fault correspondingly experienced intense subsidence, making the depression structure deeper. Similarly, the phenomenon that magma emplacement in this period can transform the early depression structure controlled by high-angle faults is also prevalent in the Zhu I and Zhu III depressions of the Pearl River Mouth Basin (Pang et al., 2021), providing strong support for the research argument.

During the rifting and depression transitional stage (T80-T70), influenced by the Zhuqiong II episode movement (Wang et al., 2011), the regional extensional stress transited into the SN direction. The rifting was significantly weakened and the crustal toughness was strengthened at this stage. Compared to the thick strata of the Wenchang formation in the downthrown wall, the strata of the Enping formation were significantly thinner. During this period, the sedimentary strata showed wedge shape under the control of boundary faults, forming a wide and gentle half-graben structure with faults to the south and strata overlapping to the north (Figure 8D). After early Oligocene (about 32 Ma), spreading occurred along the central sea basin of the South China Sea (Li et al., 2015), and the whole Pearl River Mouth Basin began to enter the post-rift differential subsidence stage. Thereafter the Baiyun sag kept subsidence after a few million years of bouncing back. In the Panyu low uplift, the thick Zhuhai-Zhujiang-Hanjiang formation was deposited by multiple episodes. Some basement faults continued to be active, but the control of faults on sedimentation was greatly weakened. The stratigraphic distribution during this period was relatively uniform (Figure 8E). The sedimentary environment of the uplift transitioned from terrestrial to marine-terrestrial and marine facies, resulting in the development of a large-scale deltaic-coastal depositional system. In the mean time, high-quality reservoir-caprock assemblages were formed under multiple sea level eustacy.

Due to the joint influence of the Qinghai-Tibet uplift, South China extrusion (Xu et al., 2003), and the Taiwan orogenic event (Yu et al., 1997), the Panyu low uplift was subjected to NEE trending dextral strike-slip stress derived from NW-SE trending compressive stress during the Neotectonic period (approximately 13.8 Ma to 5.5 Ma). On the basis of the early-formed deep fault system, a large number of nearly NW-NWW trending right-lateral left-step echelon fault belts and reverse "S" type fault zones were inheritably developed on the uplift by the arrival and compression of Philippine Sea Plate. The faults were sharply increased in number, with a maximum dominant distribution direction of N122° (Figure 7A) and an average activity rate of 15 m/s (He et al., 2019). The spatial distribution characteristics of the faults reflect that the primary extensional structure was superimposed and transformed by the extensional and strike-slip field at the late stage (Figure 8F).

6 Uplift, erosion and sedimentary strata during various stages

The latest study on the tectonic-sedimentary response of the rifted basins, such as the East Africa Rift System and the Baikal Rift (Ebinger, 1989; Guo et al., 2019; Liu et al., 2022), reveals that in

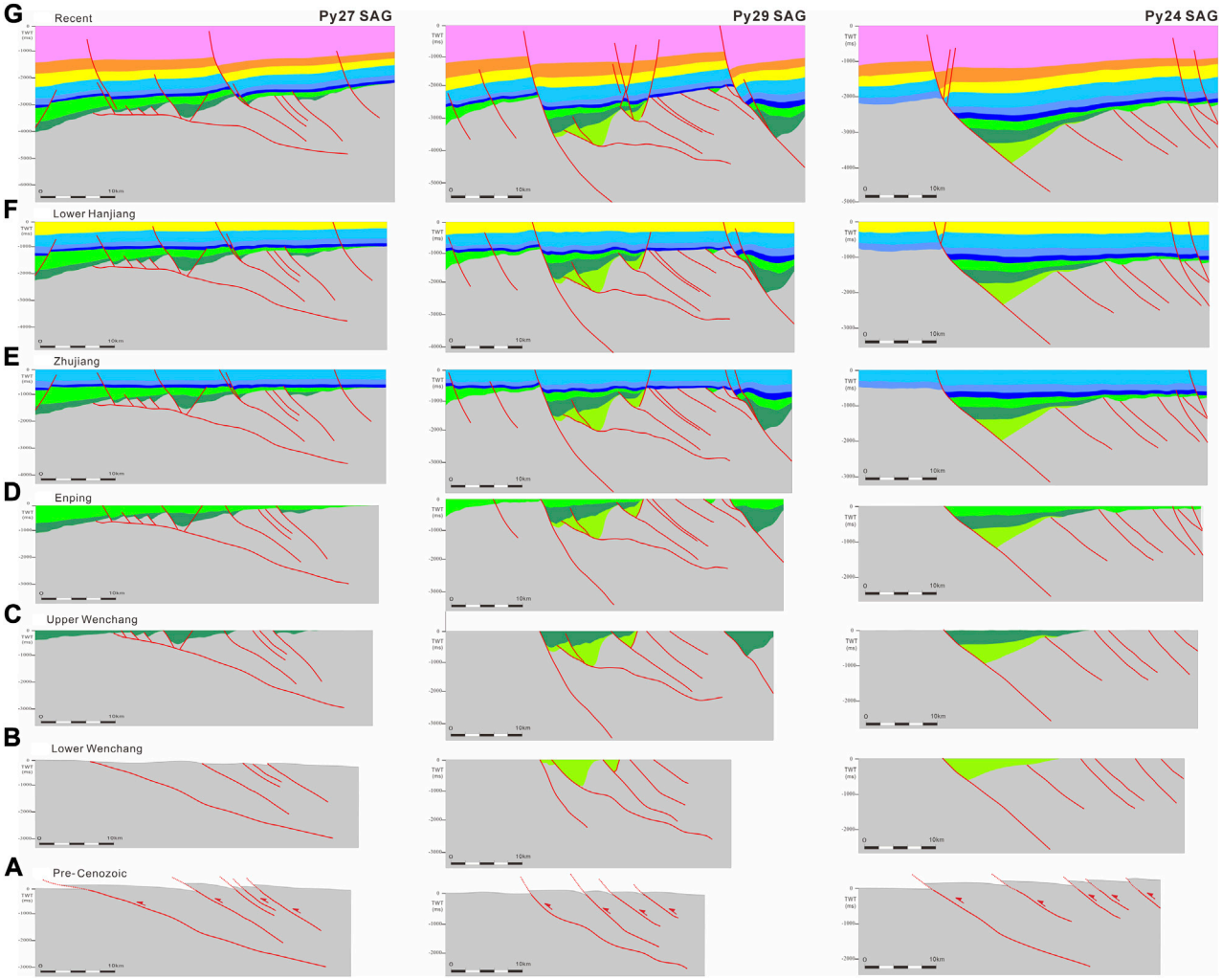

FIGURE 8
Schematic diagram delineating the tectonic evolution of the Panyu low uplift since the Pre-Cenozoic. The six main stages of deformation include: **(A)** Pre-existing compressional thrusting in the Pre-Cenozoic **(B)** Initial rifting stage during the deposition period of the Lower Wenchang formation. **(C)** Intensive rifting stage during the deposition period of the Upper Wenchang formation. **(D)** Rifting and depression transitional stage in the Late Eocene. **(E)** Thermal regional subsidence during the Oligocene to Early Miocene. **(F,G)** Tectonic reactivation in the Middle Miocene to Quaternary.

continental rift basins, the deposition and filling are controlled by the tectonic partition formed during the extension of high-angle faults. The subsidence center is distributed along the sliding direction of the main boundary faults, forming the basic sedimentary unit of half-graben. The asymmetric subsidence and sedimentary center are located in the vicinity of the boundary faults, with provenance derived from the axial direction of the rifted depression and the hanging wall. During the detachment and rifting period, compared to the extension of the early stage, the accommodation space of the rifted basin was large in depth, width, and area. The hanging wall of faults has undergone rotational tilting and intense erosion. As a result, fluvial and braided river deltas were deposited. At the same time, under-compensated large or medium-deep lacustrine sediments were deposited within the depression.

In the Panyu low uplift, there are multiple sets of NEE and NW-trending large fault systems in the basement, which control the sedimentary filling and tectonic evolution of the residual depressions. Most depressions are characterized by a half-graben structure with large controlling faults in the south and strata that overlap to the north. Based on the seismic reflection structure, lithological combination, and well logging facies, the study shows that, affected by the activities of boundary faults, the residual depression in the uplift had undergone three tectonic evolution stages during the Eocene, represented by the initial rifting stage, the intensive rifting stage, and the rifting and depression transitional stage. During the initial rifting period, the Panyu low uplift manifested as multiple segmented half-grabens. The sedimentary strata were distributed in the downthrown wall of the depression-controlling faults, exhibiting multiple subsidence and sedimentary centers. At the same time, the depression was supplied by multiple provenance systems. During the intense rifting period, the depression widened, the lacustrine basins were connected with each other, and the sedimentary center migrated. During the rifting and depression transitional stage, the control of faults on deposition weakened. The thick Enping formation from the

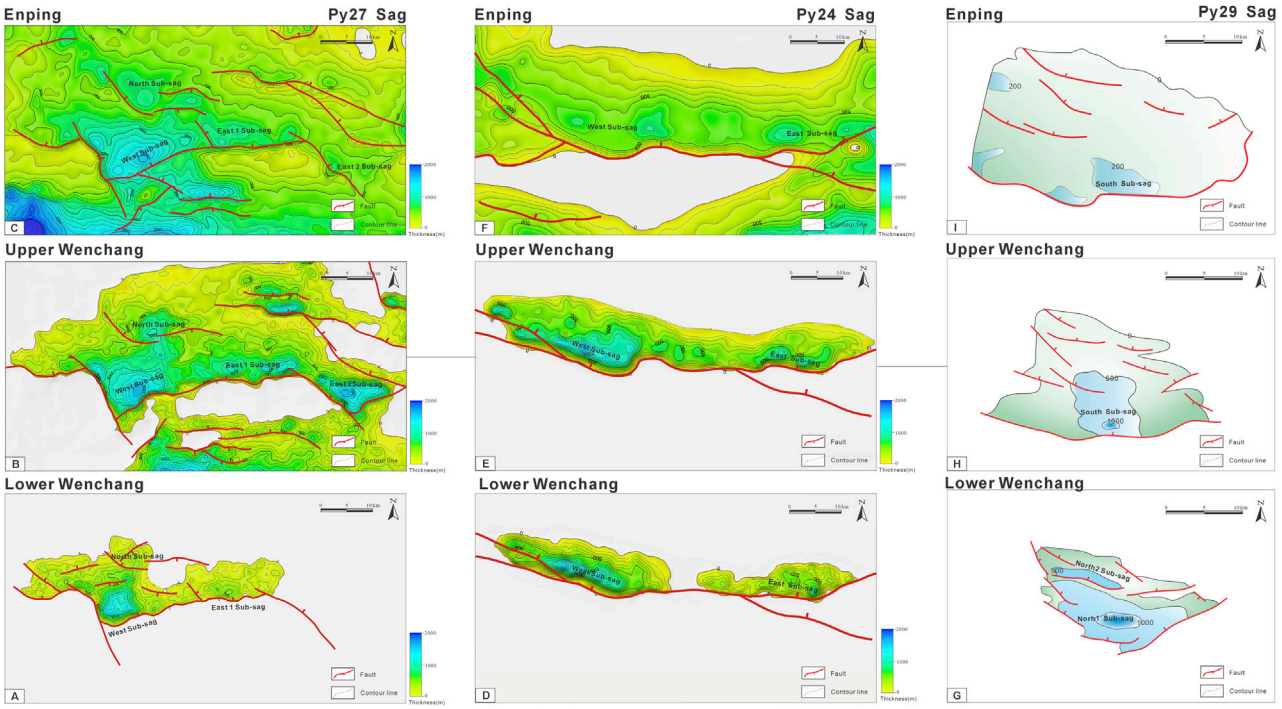

FIGURE 9
(A–F) Stratigraphic isopach maps (in two-way travel time) of the Lower, Upper Wenchang and Enping formation, which are superimposed by active fault arrays in the PY27, PY24 sags. **(G–I)** Schematic stratigraphic isopach maps (in TWT) in the PY29 sag.

northwest provenance direction is unconformably overlaid on the Panyu low uplift. Meanwhile, various types of sedimentary facies were developed in the residual depressions, including the delta, semi-deep lacustrine, shallow lacustrine, and shore-shallow lacustrine deposits. Among them, the mudstone developed in the semi-deep lacustrine and fluvioglacial swamps can serve as a high-quality hydrocarbon source rock, which has certain potential for hydrocarbon production.

In conclusion, rifting subsidence took place in the Panyu low uplift during the Eocene period. The depression in the Panyu low uplift area kept subsiding while the uplift area continued to rise. The depression was mainly featured by the lacustrine basin sediments, which developed various types of sedimentary systems of lacustrine basin, and supplied by multiple provenance from different directions.

6.1 Panyu 27 depression

The Panyu 27 depression covers an area of about 550 km^2, where the Wenchang, Enping, Zhuhai formation, and above strata are deposited. All sub-depressions, such as the western, the northern, the eastern 1, and the eastern 2 sub-depressions, show inheritance development. The western sub-depression with the thickest sedimentary strata has been the subsidence center for a long time. During the depositional period of the Wenchang formation, the depression was at the initial rifting and intensive rifting stages, where the southern boundary faults actived intensely, making the strata concentrated in the downthrown wall. As a result, multiple sedimentary centers were formed. During the deposition of the Lower Wenchang formation, the sedimentary strata were limited in extent and distributed only in the western and eastern 1 sub-depressions. The western sub-depression was controlled by both the F3 extensional fault and the F2 extensional fault with a dextral strike-slip property. During this period, the sedimentary facies were dominated by shore-shallow lacustrine deposits (Figure 9A). During the depositional period of the Upper Wenchang formation, the sedimentary range of the lacustrine basin significantly expanded. Affected by the intense activity of the F5 detachment fault and the NW trending F4 fault, the eastern 2 sub-depression had thicker formation thickness than the western sub-depression, which became the second largest subsidence center in the region. The shore-shallow lacustrine expanded (Figure 9B; Figure 11A). In the central part of the western sub-depression, the seismic reflection showed low-frequency, moderate-good continuity, and parallel sheet-like strong amplitude, which was speculated to be the sediments of semi-deep lacustrine facies and could act as high-quality source rocks (Figure 10A). Correspondingly, at the root of the southern boundary fault, the seismic reflection showed moderate-poor continuity with wedge-shaped heterogeneous features, which was presumed to be a set of fan-delta facies. Whereas at the ramp zone, medium-high frequency, moderate-poor continuity, and medium-weak amplitude seismic reflections were observed, which corresponded to the braided-river delta facies. During the depositional period of the Enping formation, the study area was in the rifting and depression transitional stages. The control of faults on stratigraphic deposition was weakened. The lacustrine basin reached its maximum range. The flood plain facies from the NW direction were wide in range, and the braided river channels

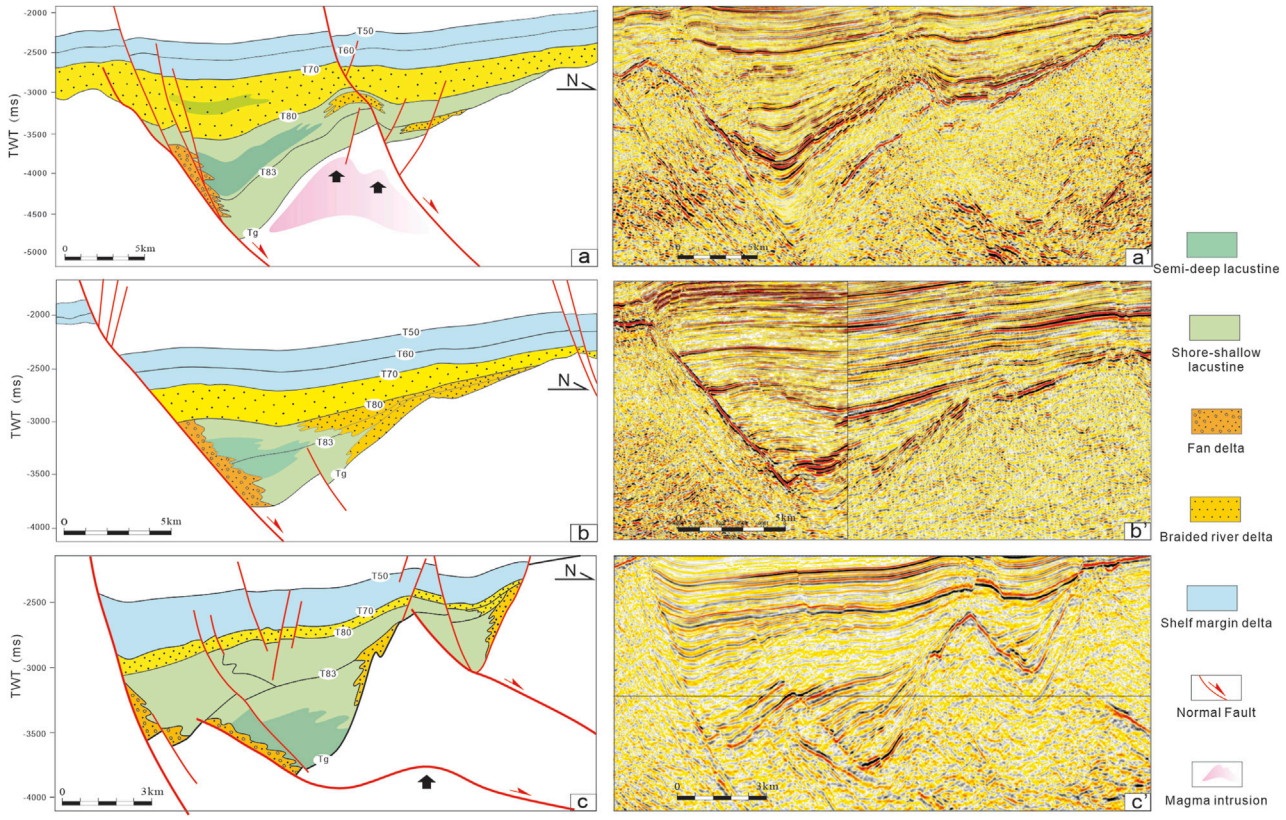

FIGURE 10
Sedimentary architecture section of **(A)** PY27 **(B)** PY24 **(C)** PY29 sags across provenance direction.

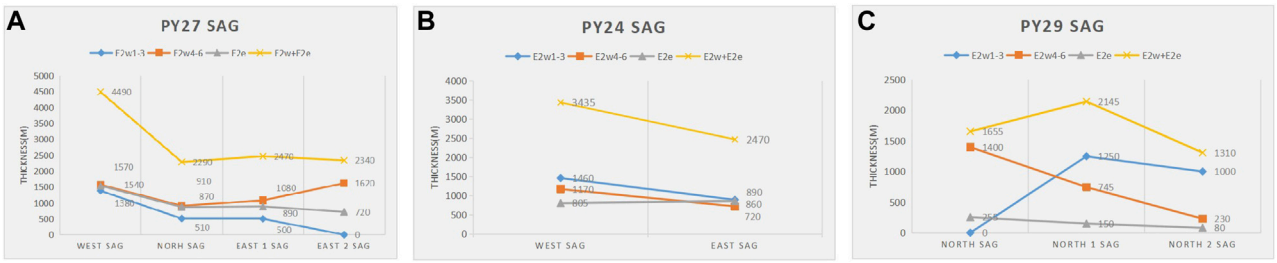

FIGURE 11
Residual thickness statistics of the Lower, Upper Wenchang and Enping formation in **(A)** PY27 **(B)** PY24 **(C)** PY29 sags for comparison. (The data are in meters transferred from two-way travel time by time-depth conversion).

from the erosion area showed flakey seismic reflection with poor continuity and moderate amplitude (Figures 9C, 10A). The swamp facies was rich in terrigenous organic matter and could also serve as an important source rock for hydrocarbons.

6.2 Panyu 24 depression

The Panyu 24 depression spans an area of approximately 460 km^2 and was influenced by multiple phases of activities of the PY24 fault. The depression exhibits a typical half-graben structure, displaying an elongated and narrow shape viewed from the plain, and is oriented in nearly an E-W direction. As such, it can be divided into both eastern and western sub-depressions. Similar to the Panyu 27 and 29 depressions, the extensional activities of the rifting stage during the Wenchang formation despositional period resulted in the concentration of strata on the downthrown side of the boundary fault. Influenced by the differential activity of the Panyu 24 fault, two separate depositional centres were developed in the footwall during the

deposition of the Lower Wenchang formation. Both of the sub-depressions were distributed in a strip-shaped pattern and parallel to the strike of the fault (Figure 9D). During the deposition of Upper Wenchang formation, the extent of the lake transgression was enlarged, and the two sub-depressions merged into a complete and large lacustrine basin (Figure 9E). Sedimentation during the rifting period was primarily dominant in the western sub-depression, resulting in a thicker stratigraphy compared to the east sub-depression (Figure 11B). The western sub-depression, showed parallel and sheet-like seismic reflections of low frequency, moderate-good continuity, and strong amplitude, which signified the deposition of semi-deep lacustrine deposits correspondingly. Meanwhile, the fan delta and braided river delta facies were developed in the southern steep slope zone and the northern ramp zone, respectively (Figure 10B). During the Enping formation's depositional period, the water became shallower and the transgressive range of the lake expanded. The sediment thickness of both the eastern and western sub-depressions was similar, and the influence of faults on stratigraphic deposition was reduced (Figures 9F, 11B). The strata in the uplifted region were eroded to provide source supply for the lower depression. A set of sedimentary filling system composed of deltaic river plain—lacustrine facies was formed in Panyu 24 depression and its surroundings. Thus, the variation of sedimentary strata and facies sequence in the Panyu 24 depression indicates an evolutionary process of water bodies transitioning from deep to shallow.

6.3 Panyu 29 depression

The Panyu 29 depression encompasses an area of around 130 km2 and exhibits a complex half-graben structure. Intense faulting occurred during the initial rifting stage where the Lower Wenchang formation deposits, with the low-angle F1 and F2 faults to the north controlling the main subsidence center. The strata in the footwall tilted and rotated, forming two sedimentary centers. The depression was both narrow and deep. The sedimentary facies were dominated by semi-deep lacustrine, characterized by parallel seismic reflections with moderate-low frequency, low continuity, and strong amplitude (Figure 9G; Figure 10C). During the depositional period of the Upper Wenchang formation, the depression-controlling fault migrated southward as the F3. At this time, the high-angle F3 fault was the dominant force controlling the deposition of the Upper Wenchang formation, and the sedimentary center of the depression migrated from north to south, causing the expansion of the lacustrine basin. Compared to the dispositional period of the Lower Wenchang formation, the water body became shallower, so shore-shallow lacustrine took dominance (Figure 9H; Figure 11C). The seismic reflections of the Enping formation were continuous and weakly deformed, but the faults still had a certain control over the deposition. From the plain view, the depression exhibits a structure of a unified large, wide, and shallow lacustrine basin. The provenance origin was from the northwest, forming a vast braided river delta and covering most of the area. Correspondingly, the seismic reflection was divergent, with moderate-weak amplitude and moderate-low continuity (Figure 9I; Figure 10C).

7 Conclusion

1. There are two major fault systems developed in the Panyu low-uplift: the deep and shallow fault systems. The deep fault system is dominated by NEE and NW-trending depression-control faults, which formed in the NW-SE and NS trending extensional stress during the Eocene. Most of them are high-angle listric or plane faults, with minor low-angle detachment normal faults under the influence of pre-existing thrust faults and magma intrusion. The shallow fault system, under the NEE trending dextral strike-slip stress field in the late Miocene, is dominated by NW-NWW trending tension-shear faults with inheritance development.
2. The tectonic evolution of Panyu low uplift can be divided into five stages, including the initial rifting stage, intense rifting stage, rifting and depression transitional stage, thermal subsidence depression stage, and tectonic reactivation stage. The faulting activities during the Eocene Zhuqiong I and Zhuqiong II episodes and the Miocene Dongsha period are the most intense.
3. Under the joint action of the long-term activity of depression-controlling faults and the pre-existing structures in the basement, the residual depressions represented by the Panyu 27, 24, and 29 depressions have relatively complex half-graben structures. During the continental rifting stage, the episodic activities of boundary faults result in the migration and inheritance of sedimentation and deposition centers in depressions, along with the changing of sedimentary sources. Besides, various types of sedimentary facies are identified, including the delta, semi-deep lacustrine, shallow lacustrine, and shore-shallow lacustrine deposits. While the mudstone of semi-deep lacustrine facies developed during the rifting period could serve as a high-quality source rock for the hydrocarbon generation.

Data availability statement

The raw data supporting the conclusion of this article will be made available by the authors, without undue reservation.

Author contributions

YL: Conceptualization, Formal Analysis, Investigation, Writing–original draft, Writing–review and editing. DY: Supervision, Writing–review and editing, Resources. SC: Supervision, Writing–review and editing. GZ: Writing–review and editing, Funding acquisition. ZB: Data curation, Writing–review and editing. XL: Conceptualization, Writing–review and editing, Data curation. YW: Investigation, Writing–review and editing. LW: Conceptualization, Writing–review and editing. SG: Conceptualization, Writing–review and editing. MJ: Writing–review and editing, Supervision. HY: Resources, Writing–review and editing.

Funding

The authors declare that this study received funding from 'Study on Grand Development Strategy of Offshore Oil and Gas

Development in the South China Sea Project' (Grants No.2022-XBZD-08-01) from the CNOOC Research Institute Ltd. The funder was not involved in the study design, collection, analysis, interpretation of data, the writing of this article, or the decision to submit it for publication.

Acknowledgments

Thanks for the contribution and support from the South China Sea East Deep Water Project Team of CNOOC Research Institute Ltd. Beijing. And we are also grateful to the reviewers and editors for their constructive suggestions, which made the paper more rigorous.

Conflict of interest

Authors YL, DY, GZ, ZB, YW, LW, SG, and MJ, were employed by CNOOC Research Institute Ltd.

The remaining authors declare that the research was conducted in the absence of any commercial or financial relationships that could be construed as a potential conflict of interest.

Publisher's note

All claims expressed in this article are solely those of the authors and do not necessarily represent those of their affiliated organizations, or those of the publisher, the editors and the reviewers. Any product that may be evaluated in this article, or claim that may be made by its manufacturer, is not guaranteed or endorsed by the publisher.

Supplementary material

The Supplementary Material for this article can be found online at: https://www.frontiersin.org/articles/10.3389/feart.2023.1281153/full#supplementary-material

References

Bahorich, M., and Farmer, S. (1995). 3-D seismic discontinuity for faults and stratigraphic features: the coherence cube. *Lead. edge* 14 (10), 1053–1058. doi:10.1190/1.1437077

Bao, H. Y., Guo, Z. F., Zhang, L. L., and Huang, Y. P. (2013). Tectonic dynamics of eastern China since the formation of the Pacific plate. *Adv. Earth Sci.* 28 (3), 337–338. doi:10.11867/j.issn.1001-8166.2013.03.0337

Briais, A., Patriat, P., and Tapponnier, P. (1993). Updated interpretation of magnetic anomalies and seafloor spreading stages in the south China Sea: implications for the Tertiary tectonics of Southeast Asia. *J. Geophys. Res.* 98 (B4), 6299–6328. doi:10.1029/92jb02280

Chen, C. M., Shi, H. S., and Xv, S. C. (2003). *Forming conditions of tertiary oiland gas reservoirsin the eastern Pearl River Mouth basin*. Beijing: Science Press.

Chen, H. Z., Wu, X. J., Zhou, D., Wang, W. Y., and Hao, H. J. (2005). Meso-Cenozoic faults in Zhujiang River Mouth basin and their geodynamic background. *J. Trop. Oceanogr.* 24 (2), 52–61. doi:10.3969/j.issn.1009-5470.2005.02.007

Cheng, S. X., Li, S. Z., Suo, Y. H., Liu, X., Yu, S., Dai, L. M., et al. (2013). Cenozoic tectonics and dynamics of basin groups of the northern South China Sea. *Mar. Geol. Quat. Geol.* 32 (6), 79–93. doi:10.3724/SP.J.1140.2012.06079

Clift, P., and Lin, J. (2001). Preferential mantle lithospheric extension under the South China margin. *Mar. Petroleum Geol.* 18 (8), 929–945. doi:10.1016/S0264-8172(01)00037-X

Dai, Y. D., Pang, X., and Li, P. L. (1998). Study on hydrocarbon accumulation in kaiping sag of Pearl River Mouth basin. *China Offshore Oil Gas Geol.* 12 (1), 12–18.

Davis, G. A., Darby, B. J., Yadong, Z., and Spell, T. L. (2002). Geometric and temporal evolution of an extensional detachment fault, Hohhot metamorphic core complex, Inner Mongolia, China. *Geology* 30 (11), 1003–1006. doi:10.1130/0091-7613(2002)030<1003:gateoa>2.0.co;2

Deng, P., Mei, L., Liu, J., Zheng, J., Liu, M., Cheng, Z., et al. (2019). Episodic normal faulting and magmatism during the syn-spreading stage of the Baiyun sag in Pearl River Mouth Basin: response to the multi-phase seafloor spreading of the South China Sea. *Mar. Geophys. Res.* 40 (1), 33–50. doi:10.1007/s11001-018-9352-9

Dong, D. D., Wu, S. G., Zhang, G. C., and Yuan, S. Q. (2008a). Exploration of the rifting process and the delay mechanism of rifting period in the deep-water basin in the northern part of the South China Sea. *Chin. Sci. Bull.* 53 (19), 2342–2351. doi:10.1360/csb2008-53-19-2342

Dong, W., Lin, C. S., Xie, L. H., Zhang, Z. T., Yang, X. F., Zhang, Y. M., et al. (2008b). Fault slope-break zone and its control over structural lithostratigraphic traps of lowstand systems tracts in southeast Panyu uplift of the Pearl River Mouth Basin. *Acta Geosci. Sin.* 30 (02), 256–262. doi:10.1016/S1003-6326(09)60084-4

Ebinger, C. J. (1989). Tectonic development of the western branch of the East Africa Rift System. *Geol. Soc. Am. Bull.* 101 (7), 855–903. doi:10.1130/0016-7606(1989)1010885:tdotwb>2.3.co;2

Gibbs, A. (1983). Balanced cross-section construction from seismic sections in areas of extensional tectonics. *J. Struct. Geol.* 5 (2), 153–160. doi:10.1016/0191-8141(83)90040-8

Gong, Z. S., Li, S. T., and Xie, T. J. (1997). *Analysis of continental margin basin and hydrocarbon accumulation in northern South China Sea*. Beijing: Science Press.

Gong, Z. S., Li, S. T., and Xie, T. J. (2004). *Dynamic research of oil and gas accumulation in northern marginal basins of South China Sea*. Beijing: Science Press.

Groshong, R. H., Jr (1989). Half-graben structures: balanced models of extensional fault-bend folds. *Geol. Soc. Am. Bull.* 101 (1), 96–105. doi:10.1130/0016-7606(1989)101<0096:HGSBMO>2.3.CO;2

Guo, R. J., Ji, H. C., Wen, Z. X., et al. (2019). The relation between tectonic activity and sedimentary frame- work: evidence from the lake albert, east african Rift System. *Mar. Geol. Front.* 35 (3), 1–12. (in Chinese with English abstract).

Hall, R. (2002). Cenozoic geological and plate tectonic evolution of SE Asia and the SW Pacific: computer-based reconstructions, model and animations. *J. Asian earth Sci.* 20 (4), 353–431. doi:10.1016/S1367-9120(01)00069-4

Han, J. H., Xu, G. Q., Li, Y. Y., and Zhuo, H. T. (2016). Evolutionary history and controlling factors of the shelf breaks in the Pearl River Mouth basin, northern South China sea. *Mar. Petroleum Geol.* 77, 179–189. doi:10.1016/j.marpetgeo.2016.06.009

Han, X. Y., Deng, S., Tang, L. J., and Cao, Z. C. (2017). Geometry, kinematics and displacement characteristics of strike-slip faults in the northern slope of Tazhong uplift in Tarim Basin: a study based on 3D seismic data. *Mar. Petroleum Geol.* 88, 410–427. doi:10.1016/j.marpetgeo.2017.08.033

He, M., Zhu, W. L., Wu, Z., Zhong, G. F., Ren, J. Y., Liu, L. H., et al. (2019). Neotectonic movement characteristics and hydrocarbon accumulation of the Pearl River mou Mouth Basin. *China Offshore Oil Gas* 31 (5), 9–20. doi:10.11935/j.issn.1673-1506.2019.05.002

Holdsworth, R., Stewart, M., Imber, J., and Strachan, R. (2001). The structure and rheological evolution of reactivated continental fault zones: a review and case study. *Geol. Soc. Lond. Spec. Publ.* 184 (1), 115–137. doi:10.1144/GSL.SP.2001.184.01.07

Jia, C. Z., Ma, D. B., Yuan, J. Y., Wei, G. Q., Yang, M., Yan, L., et al. (2022). Structural characteristics, formation and evolution and genetic mechanisms of strizke–slip faults in the Tarim Basin. *Nat. Gas. Ind. B* 9 (1), 51–62. doi:10.1016/j.ngib.2021.08.017

Li, C. F., Lin, J., Kulhanek, D. K., Williams, T., Bao, R., Briais, A., et al. (2015). Expedition 349 summary. Proceedings of the international ocean discovery program. *Int. Ocean. Discov. Program* 349, 1–43. doi:10.14379/iodp.proc.349.101.2015

Li, C. F., Xu, X., Lin, J., Sun, Z., Zhu, J., Yao, Y. J., et al. (2014). Ages and magnetic structures of the South China Sea constrained by deep tow magnetic surveys and IODP Expedition 349. *Geochem Geophys Geosyst* 15, 4958–4983. doi:10.1002/2014gc005567

Li, P. L. (1993). Cenozoic tectonic movement in the Pearl River Mouth basin. China offshore oil and gas. *Geology* 7 (6), 11–17.

Li, S. Z., Suo, Y. H., Liu, X., Dai, L. M., Yu, S., Zhao, S. J., et al. (2012). Basin dynamics and basin groups of the South China Sea. *Mar. Geol. Quat. Geol.* 32 (6), 55–78. doi:10.3724/SP.J.1140.2012.06055

Liu, B. J., Pang, X., Xie, S. W., Mei, L. F., Zheng, J. Y., Sun, H., et al. (2022). Control effect of crust-mantle detachment fault activity on deep large delta sedimentary system

in Baiyun Sag. Pearl River Mouth Basin. *Earth Sci.* 47 (7), 2354–2373. doi:10.3799/dqkx.2022.035

Liu, B. J., Pang, X., Yan, C. Z., Liu, J., Lian, S. Y., He, M., et al. (2011). Evolution of the Oligocene-Miocene shelf slope-break zone in the Baiyun deep-water area of the Pearl River Mouth Basin and its significance in oil-gas exploration. *Acta Pet. Sin.* 32 (2), 234–242. doi:10.7623/syxb201102007

Liu, H. L., Mei, L. F., Shi, H. S., Shu, Y., Tian, W., and Ye, Q. (2018). Rift style controlled by basement attribute and regional stress in Zhu I depression. Pearl River Mouth Basin. *Earth Sci.* 62 (3), 1–17. doi:10.3799/dqkx.2018.576

Liu, S. F. (2018). *Study on the distribution of basins, faults and igneous rocks by gravity and magnetic data in the South China sea*. Beijing: China University of Geosciences.

Liu, T. S., and He, S. B. (2001). Deepwater hydrocarbon potential along the north continental margin, the South China Sea. *China Offshore Oil Gas Geol.* 15 (3), 164–170.

Liu, Y. Q., Deng, S., Zhang, J. B., Qiu, H. B., Han, J., and He, S. G. (2023). Characteristics and formation mechainism of the strike-slip fault networks in the Shunbei area and the surroundings, Tarim Basin. *Earth Sci. Front.* doi:10.13745/j.esf.sf.2023.2.31

Lu, B. L., Wang, P. J., Zhang, G. C., and Wang, W. Y. (2015). Characteristic of regional fractures in South China Sea and its basement tectonic framework. *Prog. Geophys.* 30 (4), 1544–1553. doi:10.6038/pg20150408

Luo, X. G., Wang, W. Y., Zhang, G. C., Zhao, Z. G., Liu, J. L., Xie, X. J., et al. (2018). Study on distribution features of faults based on gravity data in the South China Sea and its adjacent areas. *Chin. J. Geophys.* 61 (10), 4255–4268. doi:10.6038/cjg2018L0561

Ma, B. S. (2020). *The cenozoic structural characteristics and tectonic evolution of the Pearl River Mouth basin, northern South China sea*. Beijing: China University of Petroleum.

Ma, B. S., Qi, J. F., Wu, G. H., Ren, J. Y., Yang, L. L., Sun, T., et al. (2022). Structural variability and rifting process of the segmented cenozoic Pearl River Mouth basin, northern continental margin of the South China sea. *Acta Geol. Sinica-English Ed.* 96 (6), 2074–2092. doi:10.1111/1755-6724.14983

Ma, Z. J., Qu, G. S., and Chen, X. F. (2008). Tectonic framework and division in Junggar basin. *Xinjiang Pet. Geol.* 29 (1), 1–6.

Mi, L. J., Zhang, G. C., Fu, N., He, Q., and Ma, L. W. (2006). An analysis of hydrocarbon source and accumulation in Panyu low/uplift and north slope of Baiyun sag. *Pearl River Mouth Basin* 18 (3), 161–168.

Mi, L. J., Zhang, X. T., Pang, X., Zheng, J. Y., and Zhang, L. L. (2019). Formation mechanism and petroleum geology of Pearl River Mouth basin. *Acta Pet. Sin.* 40 (s1), 1–10. doi:10.7623/syxb2019S1001

Morley, C., Haranya, C., Phoosongsee, W., Pongwapee, S., Kornsawan, A., and Wonganan, N. (2004). Activation of rift oblique and rift parallel pre-existing fabrics during extension and their effect on deformation style: examples from the rifts of Thailand. *J. Struct. Geol.* 26 (10), 1803–1829. doi:10.1016/j.jsg.2004.02.014

Ning, F., Jin, Z. J., Zhang, Z. P., Yun, J. B., and Zhang, J. B. (2018). Mechanism of strike-slip faulting and hydrocarbon accumulation in northern slope of Tazhong area. *Oil Gas Geol.* 39 (1), 98–106. doi:10.11743/ogg20180110

Pang, X., Chen, C. M., Peng, D. J., Zhou, D., Shao, L., He, M., et al. (2008). Basic geology of Baiyun deep-water area in the northern South China Sea. *China Offshore Oil Gas.* 20 (4), 215–222.

Pang, X., Chen, C. M., Shao, L., Wang, C. S., Zhu, M., He, M., et al. (2007). Baiyun movement, a great tectonic event on the Oligocene-Miocene boundary in the northern South China Sea and its implications. *Geol. Rev.* 53 (2), 145–151. doi:10.16509/j.georeview.2007.02.001

Pang, X., Ren, J. Y., Zheng, J. Y., Liu, J., Yu, P., and Liu, B. J. (2018). Petroleum geology controlled by extensive detachment thinning of continental margin crust: a case study of Baiyun sag in the deep-water area of northern South China Sea. *Petroleum Explor. Dev.* 45 (1), 29–42. doi:10.1016/S1876-3804(18)30003-X

Pang, X., Shi, H. S., Zhu, M., Yan, C., Liu, J., Zhu, J., et al. (2014). A further discussion on the hydrocarbon exploration potential in Baiyun deep water area. *China Offshore Oil Gas* 26 (3), 23–29.

Pang, X., Zheng, J. Y., Mei, L. F., Liu, B. J., Zhang, Z., Twu, Z., et al. (2021). Characteristics and origin of continental marginal fault depressions under the background of preexisting subduction continental margin, northern South China Sea, China. *Petroleum Explor. Dev.* 48 (5), 1237–1250. doi:10.1016/s1876-3804(21)60106-4

Qiu, H. B., Deng, S., Cao, Z. C., Yin, T., and Zhang, Z. P. (2019). The evolution of the complex anticlinal belt with crosscutting strike-slip faults in the central Tarim basin, NW China. *Tectonics* 38 (6), 2087–2113. doi:10.1029/2018TC005229

Ren, J. Y., and Lei, C. (2011). Tectonic stratigraphic framework of Yinggehai-Qiongdongnan Basins and its implication for tectonic province division in South China Sea. *Chin. J. Geophys.* 54 (12), 3303–3314. doi:10.3969/j.issn.0001-5733.2011.12.028

Ren, J. Y., Pang, X., Yu, P., Lei, C., and Luo, P. (2018). Characteristics and formation mechanism of deepwater and ultra-deepwater basins in the northern continental margin of the South China Sea. *Chin. J. Geophys.* 61 (12), 4901–4920. doi:10.6038/cjg2018L0558

Ru, K. (1988). The development of superimposed basin on the northern margin of the South China Sea and its tectonic significance. *Oil Gas Geol.* 9 (1), 22–31. doi:10.11743/ogg19880103

Shelton, J. W. (1984). Listric normal faults: an illustrated summary. *AAPG Bull.* 68 (7), 801–815. doi:10.1306/AD461426-16F7-11D7-8645000102C1865D

Shi, H. S., He, M., Zhang, L. L., Yu, Q. H., Pang, X., Zhong, Z. H., et al. (2014). Hydrocarbon geology, accumulation pattern and the next exploration strategy in the eastern Pearl River Mouth Basin. *China Offshore Oil Gas* 26 (3), 11–22.

Shi, H. S., Qin, C. G., Gao, P., Zhang, Z. T., Zhu, J. Z., and Zhao, R. Y. (2008). Late gas accumulation characteristics in Panyu low-uplift and the north slope of Baiyun sag, Pearl River Mouth Basin. *China Offshore Oil Gas* 20 (2), 73–76+95. doi:10.3969/j.issn.1673-1506.2008.02.001

Song, H. B., Hao, T. Y., Jiang, W. W., Qiu, X. L., Xu, Y., and Liu, J. H. (2002). Researches on geophysical field characteristics and basement fault system of South China Sea. *Prog. Geophys.* 17 (1), 24–33. doi:10.3969/j.issn.1004-2903.2002.01.003

Sun, Z., Pang, X., and Zhong, Z. H. (2005). Dynamics of tertiary tectonic evolution of the Baiyun sag in the Pearl River Mouth basin. *Earth Sci. Front.* 12 (4), 489–498. doi:10.3321/j.issn:1005-2321.2005.04.018

Sun, Z., Xu, Z., Sun, L., Pang, X., Yan, C., Li, Y., et al. (2014). The mechanism of post-rift fault activities in Baiyun sag, Pearl River Mouth basin. *J. Asian Earth Sci.* 89, 76–87. doi:10.1016/j.jseaes.2014.02.018

Wang, B. (2007). *Hydrocarbon migration pathway system of PanyuLow uplift in the Pearl River Mouth basin*. Wuhan: China University of Geosciences. doi:10.3969/j.issn.1008-2336.2006.01.001

Wang, B., Zhu, C. R., and Feng, Y. (2005). Structure ridge and hydrocarbon migration pathway system of Panyu low uplift in the pearl river mouth basin. *Offshore oil.* 26 (1), 1–6. doi:10.3969/j.issn.1008-2336.2006.01.001

Wang, J. H., Liu, L. h., Chen, S. H., and Shang, Y. (2011). Tectonic-sedimentary responses to the second episode of the Zhu-Qiong movement in the Enping depression, Pearl River Mouth basin and its regional tectonic significance. *Acta Pet. Sinica/Shiyou Xuebao* 32 (4), 588–595. doi:10.1007/s12182-011-0123-3

Wang, Z. Y., Li, H. B., Zheng, J. Y., Zhu, D. W., Yu, S., Chen, Z. M., et al. (2023). Structural evolution and its control on source-to-sink system of Panyu 27 sag in Pearl River Mouth Basin during rifting. *Oil Gas Geol.* 44 (3), 626–636. doi:10.11743/ogg20230308

Williams, G., and Vann, I. (1987). The geometry of listric normal faults and deformation in their hangingwalls. *J. Struct. Geol.* 9 (7), 789–795. doi:10.1016/0191-8141(87)90080-0

Xia, L. Y., Lin, C. S., Li, X., and Hu, Y. (2018). Characteristics of fault structures in Pearl River Mouth Basin and control effect of them on sedimentary basin. *J. Xi'an Shiyou Univ. Nat. Sci. Ed.* 35 (5), 1–8. doi:10.3969/j.issn.1673-64X.2018.05.001

Xie, G. H., Tu, K., Wang, J. W., Zhang, M., and Flower, F. J. M. (1989). Geographic distribution characteristics and diagenetic significance of lead isotope composition of Cenozoic basalts in eastern China. *Chin. Sci. Bull.* 34 (10), 772–775.

Xie, L. H., Lin, C. S., Zhou, T., Zhang, B., and Cui, L. Y. (2009). Features of paleogene episodic rifting in Huizhou fault depression in the Pearl River Mouth basin. *Natur. Gas. Ind.* 29 (1), 35–37. doi:10.3787/J.issn.1000-0976.2009.01.007

Xie, X. N., Ren, J. Y., Wang, Z. F., Li, X. S., and Lei, C. (2015). Difference of tectonic evolution of continental marginal basins of South China Sea and relationship with SCS spreading. *Earth Sci. Front.* 22 (1), 77–87. doi:10.13745/j.esf.2015.01.007

Xu, J., Ma, Z. j., and Chen, G. g. (2003). NW trending active fault zones of the eastern Chinese continent in neotectonic time. *Earth Sci. Front.* 10 (Suppl. P), 193–198. doi:10.3321/j.issn:1005-2321.2003.z1.027

Xue, C., Zhang, S. F., and Du, J. Y. (2012). PY24 fault through Panyu low-uplift of pearl river mouth basin: characteristics and impact on sedimentation. *Mar. Geol. Front.* 28 (6), 10–14. doi:10.16028/j.1009-2722.2012.06.009

Ye, Q. (2019). *The late mesozoic structure systems in the northern South China sea margin: geodynamics and their influence on the cenozoic structures in the Pearl River Mouth basin*. Wuhan: China University of Geosciences.

Ye, Q., Mei, L. F., Shi, H. S., Shu, Y., Camanni, G., and Wu, J. (2018). A low-angle normal fault and basement structures within the enping sag, Pearl River Mouth basin: insights into late mesozoic to early cenozoic tectonic evolution of the South China sea area. *Tectonophysics* 731, 1–16. doi:10.1016/j.tecto.2018.03.003

Yu, S. B., Chen, H. Y., and Kuo, L. e. (1997). Velocity field of GPS stations in the Taiwan area. *Tectonophysics* 274 (1-3), 41–59. doi:10.1016/S0040-1951(96)00297-1

Yu, S. M., Mei, L. F., Shi, H. S., Qin, C. G., and Tang, J. G. (2007a). Relationship between faults and hydrocarbon accumulation in Panyu low massif and north slope of Baiyun sag, Pearl River Mouth Basin. *Petroleum Explor. Dev.* 34 (5), 562–565+579. doi:10.1016/S1872-5813(07)60034-6

Yu, X. H., Jiang, H., Shi, H. S., and Hou, G. W. (2007b). Study on depositional characteristic and diagenetic evolvement in Panyu gas field of Peal River Mouth Basin. *Acta Sedimentol. Sin.* 25 (6), 876–884. doi:10.14027/j.cnki.cjxb.2007.06.014

Zhang, G. C. (2010). Tectonic evolution of deepwater area of northern continental margin in South China Sea. *Acta Pet. Sin.* 31 (4), 528–533. doi:10.7623/syxb201004002

Zhang, G. C. (2023). Theory of deepwater hydrocarbon accumulation controlled by progressive tectonic cycles of marginal sea in the South China Sea. *Acta Pet. Sin.* 44 (4), 569–582. doi:10.7623/syxb202304001

Zhang, G. C., Jia, Q. J., Wang, W. Y., Wang, P. J., Zhao, Q. L., Sun, X. M., et al. (2018). On tectonic framework and evolution of the South China Sea. *Chin. J. Geophys.* 61 (10), 4194–4215. doi:10.6038/cjg2018L0698

Zhang, G. C., Yang, H. Z., Chen, Y., Ji, M., Wang, K., Yang, D. S., et al. (2014). The Baiyun sag: a giant rich gas-generation sag in the deepwater area of the Pearl River Mouth Basin. *Natur. Gas. Ind.* 34 (11), 11–25. doi:10.3787/j.issn.1000-0976.2014.11.002

Zhang, S. F., Zhang, X. T., Zhang, Q. L., and She, Q. H. (2015). Characteristics of the cretaceous in the northern South China Sea and tectonic implications. *Mar. Geol. Quat. Geol.* 35 (6), 81–86. doi:10.16562/j.cnki.0256-1492.2015.06.008

Zhang, Z. T., Qin, C. G., Gao, P., Qu, L., Liu, D. L., and Xuan, Y. H. (2011). Accumulation of natural gas and main controlling factors in PY-LHzone in Zhujiang River Mouth basin. *Nat. Gas. Geosci.* 22 (5), 778–783.

Zhao, Z. X., Zhou, D., and Liao, J. (2009). Tertiary paleogeography and depositional evolution in the Pearl River Mouth basin of the northern South China sea. *J. Trop. Oceanogr.* 28 (06), 52–60. doi:10.3969/j.issn.1009-5470.2009.06.007

Zheng, J. Y., Gao, Y. D., Zhang, X. T., Pang, X., Zhang, Q. L., Lao, M. J., et al. (2022). Tectonic evolution cycles and cenozoic sedimentary environment changes in Pearl River Mouth Basin. *Earth Sci.* 47 (7), 2374–2390. doi:10.3799/dqkx.2021.258

Zhong, Z. H., Shi, H. S., Zhu, M., Pang, X., He, M., Zhao, Z. X., et al. (2014). A discussion on the tectonic-stratigraphic framework and its origin mechanism in Pearl River Mouth Basin. *China Offshore Oil Gas* 26 (5), 20–29.

Zhou, D., Chen, H. Z., Wu, S. M., and Yu, H. S. (2002). Opening of the South China sea by dextral splitting of the East asian continental margin. *Acta Geol. Sin.* 76 (2), 180–190.

Zhou, D., Sun, Z., and Chen, H. Z. (2005a). Mesozoic lithofacies, paleo-geography, and tectonic evolution of the South China Sea and surrounding areas. *Earth Sci. Front.* 12 (3), 204–218. doi:10.3321/j.issn:1005-2321.2005.03.022

Zhou, D., Wang, W. Y., Wang, J. L., Pang, X., Cai, D. S., and Sun, Z. (2006). Mesozoic subduction-accretion zone in northeastern South China Sea inferred from geophysical interpretations. *Sci. China Ser. D* 49 (5), 471–482. doi:10.1007/s11430-006-0471-9

Zhou, D., Wu, S. M., and Chen, H. Z. (2005b). Some remarks on the tectonic evolution of Nansha and its adjacent regions in southern South China Sea. *Geotect. Metallogenia* 29 (3), 339–345. doi:10.16539/j.ddgzyckx.2005.03.008

Zhou, D., and Yao, B. C. (2009). Tectonics and sedimentary basins of the South China sea: challenges and progresses. *J. Earth Sci.* 20, 1–12. doi:10.1007/s12583-009-0001-8

Zhu, J. Z., Jiang, A. Z., Shi, H. S., Sun, Y. G., Pang, X., et al. (2012). The effective gas-source area and gas migration-accumulation model in LW3-1 gas field, Baiyun sag deep water area, Pearl River Mouth Basin. *China Offshore Oil Gas* 24 (4), 25–31.

Zhu, W., and Lei, C. (2013). Refining the model of south China sea's tectonic evolution: evidence from yinggehai-song hong and qiongdongnan basins. *Mar. Geophys. Res.* 34, 325–339. doi:10.1007/s11001-013-9202-8

Zhu, W. L., Wu, J. F., Zhang, G. C., Ren, J. Y., Zhao, Z. G., Wu, K. Q., et al. (2015). Discrepancy tectonic evolution and petroleum exploration in China offshore Cenozoic basins. *Earth Sci. Front.* 22 (1), 88–101. doi:10.13745/j.esf.2015.01.008

Zhu, W. L., Zhong, K., Li, Y. C., Xu, Q., and Fang, D. Y. (2012). Characteristics of hydrocarbon accumulation and exploration potential of the northern South China Sea deep-water basins. *Chines Sci. Bull.* 57 (20), 3121–3129. doi:10.1007/s11434-011-4940-y

Zong, Y., Liang, J. S., and Guo, G. (2012). Characteristic of fault activity in Wenchang formation of Panyu low uplift, Pearl river mouth basin, and its influence on sedimentation. *J. Earth Sci. Environ.* 34 (4), 30–35. doi:10.3969/j.issn.1672-6561.2012.04.004